Investigation of turbulence rotation in the SOL and plasma edge of W7-X for different magnetic configurations

A. Krämer-Flecken[1*], S.A. Bozhenkov[3], G. Anda[2], D. Dunai[2], G. Fuchert[3], J. Geiger[3], O. Grulke[3], X. Han[1,5], M. Otte[3], E. Pasch[3], E.R. Scott[3], E. Trier[4], M. Vécsei[2], T. Windisch[3], S. Zoletnik[2] and the W7-X team[1]

[1] Institut für Energie- und Klimaforschung, Forschungszentrum Jülich GmbH, 52425 Jülich, Germany

[2] Wigner Research Centre for Physics, 1525 Budapest, Hungary

[3] Max Planck Institut für Plasmaphysik, 17491 Greifswald, Germany

[4] Max Planck Institut für Plasmaphysik, 85748 Garching, Germany

[5] Institute of Plasma Physics, Chinese Academy of Sciences, Hefei 230031,People's Republic of China

[*] Corresponding author A. Krämer-Flecken: a.kraemer-flecken@fz-juelich.de

Abstract:

The W7-X stellarator is optimized for neoclassical transport and turbulent transport plays an important role. It is equipped with a inertial cooled Graphite divertor which intersects, depending on the magnetic configuration the island chain at the plasma edge. Additional control coils and the plasma current modify the iota profile at the plasma edge and shift the position of the island chain. To monitor the effects on the poloidal propagation velocity in the scrape off layer (SOL) and the plasma edge an O-mode Poloidal Correlation Reflectometer is used which simultaneously monitors the propagation of low k-turbulence. Operating in the density range $0.6 \times 10^{19}\,\mathrm{m}^{-3}$ to $2 \times 10^{19}\,\mathrm{m}^{-3}$ it covers a large part of the SOL and the plasma edge and allows in low to medium density discharges to determine experimentally the last closed flux surface (LCFS) and the associated shear layer.

In this paper it is shown that the propagation in the shear layer and its vicinity is determined best, when based on an elliptical model. Different magnetic configurations having an edge iota of $\iota = 1$ and $\iota = 0.81$ are investigated. Also the effects of the plasma current and additional control coils on the edge magnetic topology are studied.

[1]Author list Nuclear Fusion Vol. 53 No. 12 Article 126001 (2013)

The coherence spectra of antenna pairs for different poloidal separations is investigated. Using a decomposition method for the measured coherence spectra the characterization of turbulence spectra is possible with respect to e.g. broad band turbulence and quasi coherent modes. A strong reduction of the broad band turbulence is observed in the vicinity of the LCFS which is evidence for the suppression of low k turbulence at the shear layer.

Keywords: stellarator, correlation reflectometer, turbulence rotation, scrape off layer, last closed flux surface

(Some figures may appear in colour only in the online journal)

1 Introduction

The plasma edge and the scrape off layer (SOL) are important regions in any fusion device. They isolate the well confined core plasma from the divertor and first wall. Energy, if not radiated, and particles have to pass this region to reach the divertor plates. The last closed flux surface (LCFS) is the interface between the still confined plasma edge with long connection length in the order of kilometre and the SOL where the connection length is less than 100 m. In this region the plasma rotation as well as the radial electric field changes sign generating a strong shear layer. This influences the propagation of small scale structures which are expected to be torn apart by the shear. In addition the mean gradients of density and temperature change a lot in this region which influences the properties of microscopic structures [1, 2]. Furthermore it gives rise for different kinds of modes as ion temperature gradient modes and ballooning modes. For this reason the knowledge of rotation $v_\perp$- and E_r-profiles are of interest, because they determine the radial transport.

Regarding the tools used for probing these regions, diagnostics using micro waves are highly appreciated because they can be operated continously during a dischare and do not perturb the plasma. Reflectometry with a high sampling rate is a suitable choice as long as the density fluctuation level is small enough allowing the assumption of a reflection at plasma cut off density (rough mirror). However, when the density fluctuation become larger the effects of small angle scattering will disturb the measurements [3]. With a two point measurement along the poloidal direction the estimation of the plasma rotation is possible. However, every poloidal correlation measurement implies a radial correlation as well due to the radial extension of the structure. In the vicinity of a shear layer this effect could mask the real estimation of the velocity profile in the shear layer. Therefore two methods are used. One based on the measurement of the delay time of two point measurements from the cross correlation, only. The second one is based on the so called elliptical model based on earlier work by Briggs [4], Phillips [5] and Conway [6]. The different methods are compared in this paper.

The experiments reported here are performed at the superconducting stellarator W7-X [7, 8]. W7-X is optimized for neoclassical transport and has a 5 fold symmetry. In each of the 5 modules the plasma cross section varies from bean shape to triangular shape. W7-X is equipped with an inertial cooled divertor and intersects

the 5/5 island chain which id for the $\iota = 1$ configuration located at the transition from the plasma edge to the SOL. An O-mode Poloidal Correlation Reflectometer (PCR) [9, 10] is installed in the bean shaped plane to measure the rotation ($v_\perp$) profiles in the plasma edge and the SOL. In the configuration with a 5/5 island chain in the SOL the influence of plasma current and additional control coils which are supposed to change size and position of the edge island chain is investigated. For different magnetic configurations (different iota profiles) the rotation profiles are estimated.

The last part of the paper discussed changes of the coherence spectrum estimated from two antennae in the vicinity of the LCFS looking for the assumed turbulence suppression of low wave number turbulence in the vicinity of a shear layer.

2 Methodology

The used correlation reflectometer [9, 10] consists of two antenna columns next to each other, a left one with 3 antenna where the middle antenna is the launcher. In this column the upper antenna is labled **B** and the lower **C**. This antenna pair has the largest poloidal separation. The right column with 2 antenna labled **D** (upper) and **E** (lower). Together four receiver antenna are available yielding six different antenna combinations.For the estimation of the $v_\perp$-profiles from correlation reflectometry to requirements are needed - (i) the measurement of the delay times from antenna combinations and (ii) a knowledge of the radius of the measurement. To obtain $v_\perp$ from a correlation reflectomter the delay time (Δt) from different independent antenna combinations (different poloidal separation z) is calculated via the cross correlation. Without a shear layer the propagation is determined from the slope of the $\Delta t - z$ diagram [11]. In case a shear layer is crossed the measured $v_\perp$-profile is also influenced by a small radial propagation. A radial propagation of coherent structures in the SOL was reported at $\approx 10\,\%$ of the ion sound speed [12]. In fig.1 the evolution of Δt for 4 antenna combinations is shown in the shear layer of W7-X. In this case the reflectometer is in hopping operation and the probing frequency of the reflectometer is increased every 20 ms by 0.5 GHz. The expected change in the sign of Δt due to the shear layer is observed at different times for different antenna combinations. The mean poloidal distance averaged for the scan

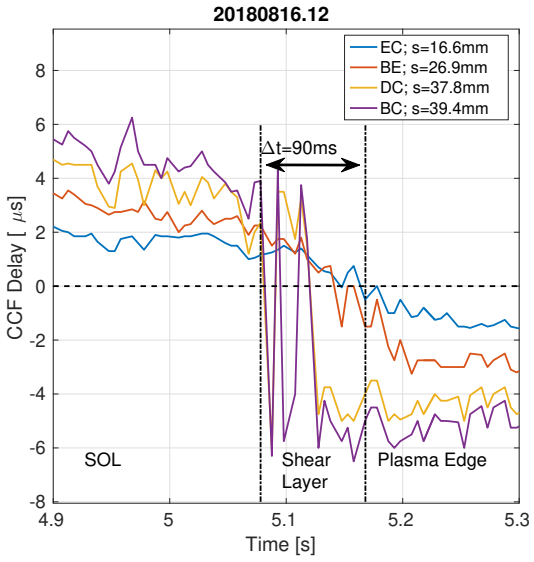

Figure 1: *Evolution of the delay times in the vicinity of the shear layer for different antennae combinations as function of time. Larger poloidal distances show an earlier flip in the delays compared to shorter ones.*

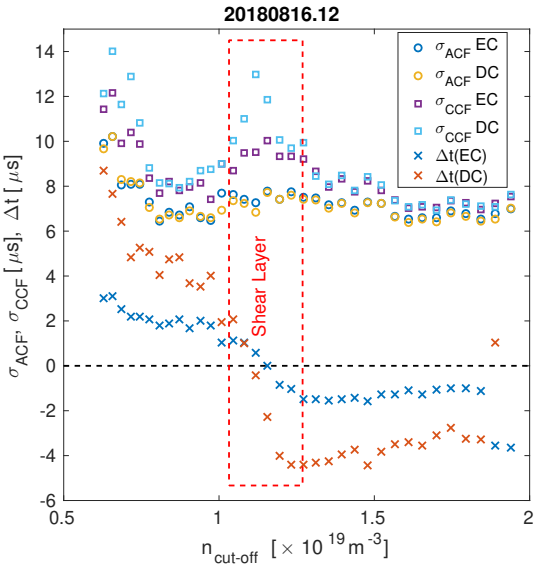

Figure 2: *Widths of auto- and cross correlation function for two antenna combination and corresponding delay for* $3.24\,\mathrm{s} \leq t \leq 3.98\,\mathrm{s}$. *Note the strong increase in the CCF width in the shear layer.*

which is partly shown in fig.1 is given in the figure as well. This observation is found in the so called standard configuration having an edge iota of $\iota = 1$ and a 5/5 island chain. As can be seen from the figure the transition happens earlier for larger poloidal distances than for smaller ones. The linear regression method applied for all six antenna combinations yields in this case a to large velocity because Δt values for the largest separation are already negative whereas for the smaller ones the delays are still positive. This behaviour clearly shows that this method will cause artificial large velocities in the shear layer. A possible explanation for this observation is found when analysing the width of the Gaussian functions used to approach the auto- and cross correlation in the delay time estimation. In fig. 2 the width of the auto correlation function (σ_{ACF}) and the cross correlation function (σ_{CCF}) are shown as function of the cut-off density. In addition the delay time for the combinations **EC** and **DC** are shown. In general both widths σ_{ACF} and σ_{CCF} yield similar values as long there is no change in the delays. However, in a narrow region the σ_{CCF} becomes nearly twice as large as σ_{ACF} for the combinations which probe a large poloidal separation e.g. combination **DC**. Furthermore, the shape of the CCF is no longer

symmetric with respect to the maximum and exhibits an asymmetric shape. An asymmetric cross correlation function is evidence that the dominate structure undergoes a significant change in its size [13]. In this case the cross correlation measures two structures, one moving with positive delays whereas the other one has negative delays. The measured time series from the antennae is a combination of both structures and the amplitude of the structure decides on the height in the CCF. As a consequence the measured σ_{CCF} becomes broader. It is therefore necessary to use a better method taking into account the width of the ACF and CCF and which can be applied in the shear layer as well. The elliptical model invented by Briggs [4] and Phillips [5] and applied for in the interpretation of plasma or fluid instabilities [6] and for turbulent shear flows by He [14] based on the assumption that iso-correlation surfaces have elliptical shape and allow to relate the cross correlation obtained for a certain Δt and a poloidal distance s to the auto correlation at a certain time lag τ. In this model the propagation velocity is given as:

$$v_\perp(x,y) = \frac{s_{xy}\Delta t_{xy}}{\Delta t_{xy}^2 + \tau_{xy}^2}; \quad x,y \in [B,C,D,E] \qquad (1)$$

From the equ. 1 it is seen, that the real drift velocity is close to the apparent velocity when $\tau \ll \Delta t$. This yields for each analysed time interval which is the hopping step width 6 values for $v_\perp$ according to the 6 antenna combinations. In fig. 3 both methods, the apparent velocity from the linear regression of the cross correlation delays and the real drift velocity using equ. 1 are compared during one frequency scan of the reflectometer. It can be seen that the estimation of $v_\perp$ in the shear region is smoother compared to the linear regression analysis. Also away from the shear layer the values of both methods are close to each other again.

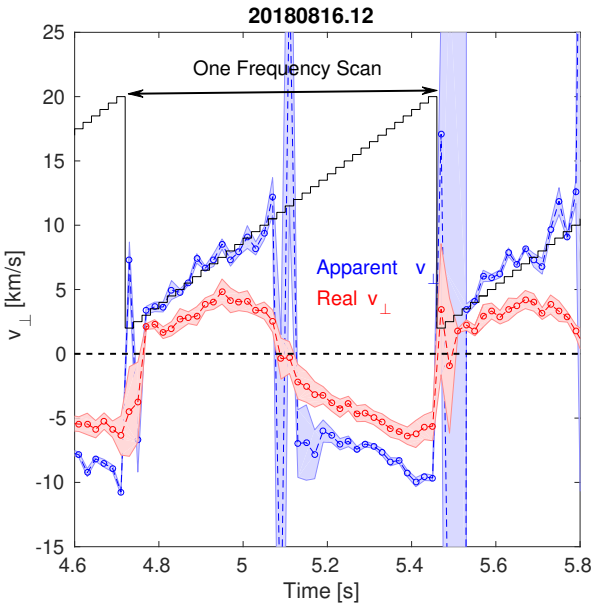

Figure 3: *Comparison of apparent and real $v_\perp$ during one frequency scan. The transition in the shear layer is no longer fluctuating and real $v_\perp$ is quite close to the $v_\perp$ to the apparent one.*

To obtain the poloidal distance on a certain flux surface defined by a certain cut-off density n_c the density profile from Thomson scattering diagnostic [15] is used. In contrast to a tokamak a stellarator has no toroidal

symmetry. PCR and Thomson scattering (TS) are located at different toroidal positions. Therefore, the effective radius r_{eff} is used for mapping inside the LCFS. Outside the LCFS the distance of the outermost TS channels with respect to the last one inside the LCFS is added. This procedure is justified for the position of the TS diagnostic, but, it is not appropriate to map the density profile to the position of the PCR because temperature and density are no longer constant on the flux surface in the SOL. The mapping becomes furthermore difficult due to the fact that the sight lines of the PCR system and the Thomson scattering diagnostic intersect the edge island, differently. Whereas the island is not intersected by the TS sight line due to changes of either planar coil- or bootstrap currents where already small currents in the planar coils can cause an increase of the 5/5 island in the line of sight of the PCR. In how far the island is large enough to cause an significant perturbation of the density profile at he position of the PCR cannot be determined. This results in an uncertainty in the estimation of radial positions outside the LCFS. For the observations in the paper it is therefore decided to use instead of r_{eff} the cut-off density as abscissa for the $v_{\perp}$-profiles.

3 Observations

The above described method is applied first for the so called standard configuration of W7-X which is characterized by an edge iota ($\iota = 1$) and has a 5/5 island chain in the SOL. The island chain is intersected by divertor plates and only small remnant island are found in the SOL. At the toroidal position of the PCR the line of sight generally intersects the island. However, as long as the density in the island is below the smallest cut-off density the measurement is not perturbed. Due to (i) the toroidal current (I_p) and (ii) additional control coils (2 per module) the edge iota changes and the position and size of the remnant island changes. In fig. 4 the important properties for the further discussion of the measurement of 3 discharges are shown. In fig. 4a the heating power and the radiated fraction is shown. It is the same for all investigated discharges as well as line integrated density shown in fig. 4b. fig. 4c shows the evolution of the plasma current which is similar for all discharges and the evolution of the control coil current (I_{cc}). For discharge 20180816.11 and 20180816.12 the I_{cc} is zero up to $t = 6\,\mathrm{s}$ Thereafter it is ramped with $|dI_{cc}/dt| = 150\,\mathrm{A\,s^{-1}}$ up (20180816.11) and down (20180816.12),

respectively. A third discharge (20180816.13) is investigated where one half of the coils have a positive and the other half a negative current ramp rate. The absolute current ramp rate is in all coils equal. In a first step the influence of I_{cc} on $v_\perp$-profile is investigated. In fig. 5 the $v_\perp$-profile as function of the cut-off density is shown. The investigated range of density covers the plasma edge and the SOL region, but not the remnant 5/5 island structure. For the investigated time range the averaged plasma current amounts to $\langle I_p \rangle = 7.4\,\mathrm{kA}$ for all three discharges. A clear transition between negative and positive $v_\perp$, forming the shear layer, can be observed. At those densities where $v_\perp$ starts to increase the LCFS is localized. Since the configuration for all three plasmas are equal the LCFS as calculated from the VMEC-equilibrium is located at $r_{LCFS} = 0.512\,\mathrm{m}$. Negative values in $v_\perp$ are obtained in the plasma edge where the connection length are long, whereas $v_\perp$ becomes positive in the SOL. Beside the three profiles with different I_{cc} the $\times$-symbols denote the mean profile as obtained in the time range 3.28 s to 3.96 s where no I_{cc} is applied and $\langle I_p \rangle = 2.9\,\mathrm{kA}$ is measured. Within the error bar of the measurement there is no difference between the case w/o, positive and alternating I_{cc}. In the plasma edge $n_c > 1.5 \times 10^{19}\,\mathrm{m}^{-3}$ no difference in $v_\perp$ is found. However, the transition from negative to positive $v_\perp$ happens at a higher density for the case with negative I_{cc}. The transition itself is

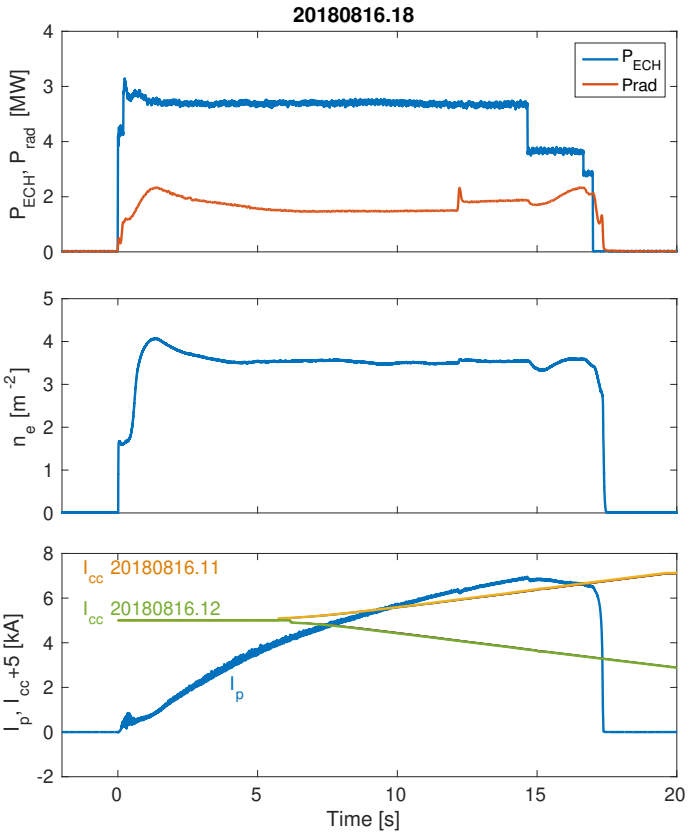

Figure 4: *Overview of I_{cc}-scan. [**a**] P_{ECH} and P_{rad}; [**b**] line averaged density; [**c**] plasma and control coil current. Note the latter has an offset of* 5 kA *for better comparison with I_p. P_{ECH}, P_{rad}, n_e and I_p are shown for 20180816.18, only for clearness.*

much steeper than in the other cases implying a larger shearing rate for this case. Because r_{LCFS} is fixed for all three discharges the observation show evidence for large changes in the edge density profile. In the SOL the $v_\perp$ profile for $-I_{cc}$ exhibits lower values than in the other discharges. In general it can be concluded that the application of I_{cc} will mainly affect the SOL whereas the $v_\perp$ in the plasma edge is unchanged. Furthermore the results suggest that the effect of the plasma current and $+I_{cc}$ seems to cancel each other.

In addition to the effect of I_{cc} the effect of the plasma current is studied. A plasma with strong increase in I_p is investigate at slightly different plasma parameters. The obtained profile is shown in fig. 6 for five different values of I_p, which is the averaged value in of the depicted time range. Again a transition from negative to positive $v_\perp$ is found. Due to the lower line averaged density the PCR measures deeper in the plasma which results in a wider range with negative $v_\perp$ in the plasma edge. In this plasma the PCR is triggered 2.5 s after plasma start and therefore the lowest plasma current is $\langle I_p \rangle = 4.4\,\mathrm{kA}$. First effect in the $v_\perp$ profile are seen at $\langle I_p \rangle = 8.1\,\mathrm{kA}$ where the transition from negative to positive $v_\perp$ becomes more steep. With increasing I_p the transition stays steep but it moves to higher densities. Such an behaviour is expected because the increase of I_p goes along with an increase of the poloidal magnetic field. Therefore, iota at the plasma edge is increased and the island structure is shifted more inward.

As mentioned before a 5/5 island chain is located in the SOL for the standard configuration. In a few cases, when the island size is small or a density peaking is observed in the remnant island it is possible to measure the rotation profile in the island. However, flat or hollow profiles cannot be detected by the PCR because it is operated in O-mode polarization. For the discharge 20180814.47 the line integrated density was that high ($5 \times 10^{19}\,\mathrm{m}^{-3}$) that the PCR diagnostic could cover the remnant island in the SOL. At the island position the connection length increases and a small well defined region is created with good confinement. In this region the sign of $v_\perp$ changes again [16]. Three different scans are analysed at different I_p values to study the effect of the plasma current on the island. As shown in fig. 7 a region of negative $v_\perp$ is found for a density range $1.23 \times 10^{19}\,\mathrm{m}^{-3}$ to $1.43 \times 10^{19}\,\mathrm{m}^{-3}$. In this region the connection length is supposed to increase which yields negative $v_\perp$. However, the increase I_p will have no effect on the density inside the remnant island. Furthermore the shape of the profile in the vicinity of the island supports the assumption that the island forms a shoulder in

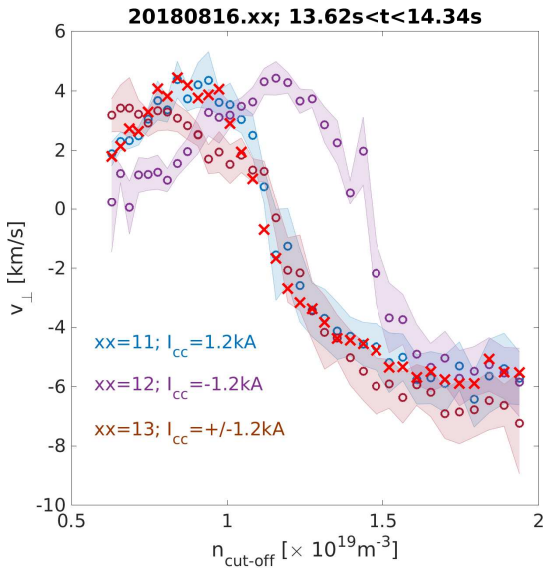

Figure 5: *$v_\perp$-profile for 20180816.11,12 and 13 showing the effect of an additional control coil current. Red X-symbols denote the mean $v_\perp$ profile without I_{cc} but different I_p.*

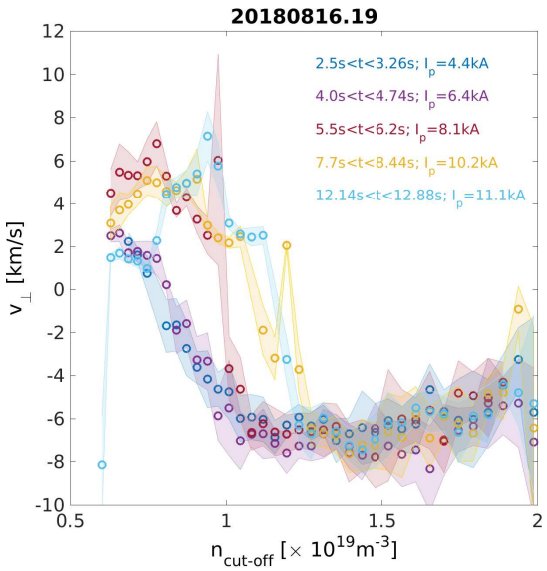

Figure 6: *$v_\perp$-profile for 20180816.19. The different profiles indicate the effect plasma current on $v_\perp$. After a steepening of the transition to the SOL a further increase in I_p shifts the transition to higher cut off densities.*

the density profile because of the smooth transition of the profile at the inner and outer island separatrix.

Beside the effect of plasma- and control coil current on the $v_\perp$-profile in the SOL it is of interest to compare the bahaviour of the $v_\perp$-profile for different magnetic configurations and plasma parameter. Therefore a set of discharges is analysed with similar line averaged density to ensure that the measurement of the PCR covers the SOL and plasma edge, respectively. In the low iota configuration ($\iota = 0.81$ at the LCFS) three discharges are used having power levels of 2 MW, 3.5 MW and 5 MW. The analyzed scan is the same in all three plasmas to keep effects of the plasma current small and to avoid pertbations by I_p-effects as discussed above. For the standard configuration ($\iota = 1$ at the LCFS) a similar discharge is found where a power scan with levels of 0.8 MW, 1.9 MW, 3.2 MW and 5.1 MW is performed. In this discharge the plasma current varies with time, but, with $\langle I_p \rangle \leq 4.9$ kA does not exceed values for which at the PCR position a change of the shear layer is obsered (see fig 6). The shape of the density profiles in both configurations and during the different power steps are similar. The radius of the LCFS is estimated from VMEC-code [17] and amounts to 0.517 m in low iota

and 0.515 m in the the standard configuration. The $v_\perp$-profiles as function of the cut-off density are presented in figs. 9,8. In both configurations the influence of the power level is clearly observed. However, in the low iota configuration the transition from the plasma edge to the SOL moves to smaller densities with increasing P_{ECH}. In the standard configuration the transition moves to smaller densities, but, with decreasing P_{ECH}. In both configurations and independent from P_{ECH} the $v_\perp$ values show no variation in the SOL. The scatter in the low iota configuration may be attributed to the larger variation in the density profiles for the investigated discharges. Furthermore in this configuration $v_\perp$ is significantly smaller ($0.4\,\mathrm{km\,s^{-1}}$ to $1.3\,\mathrm{km\,s^{-1}}$) than in the standard configuration. In the plasma edge $v_\perp$ seems to be independent from the configuration and the power level and values in the range of $-6\,\mathrm{km\,s^{-1}}$ to $-4\,\mathrm{km\,s^{-1}}$ are found. Regarding the transition from the plasma edge to the SOL evidence for a reduction in the density range where the transition takes place is found when the transition moves towards smaller densities.

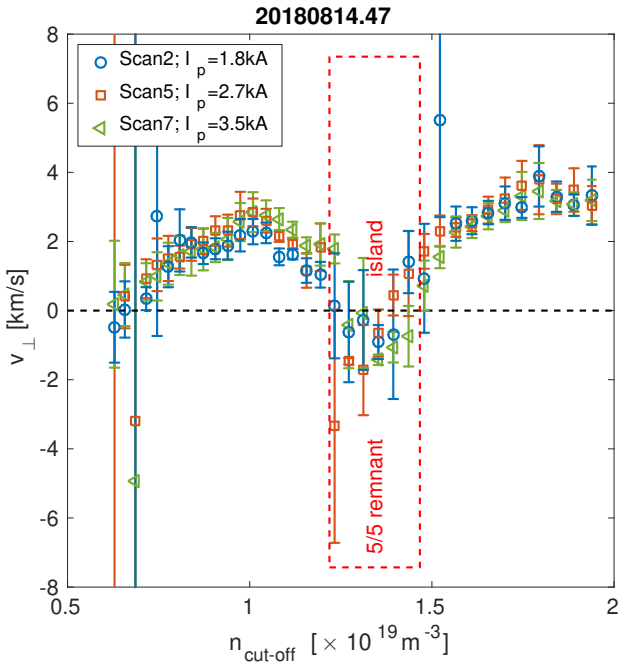

Figure 7: *$v_\perp$-profile as function of n_c for three different values of I_p. In all three cases a region with negativ $v_\perp$ values is seen and highlighted by the dashed rectangular. This region is supposed to form the remnant island.*

The LCFS is a narrow radial region where (i) the connection length decreases abruptly and the propagation velocity changes sign. The LCFS acts as a barrier for turbulent transport due to the velocity shear. It is assumed that the low wave number (k) turbulence decreases at the shear layer. A measure for the decrease of the low k-turbulence is the shearing rate ($\omega' = \partial v_\perp/\partial r$). In case the turbulence de-correlation time (τ_{dc}) exceeds the inverse shearing rate it will effectively suppressed. The PCR diagnostic is in general sensitive to low k-turbulence up to $k \approx 4\,\mathrm{cm^{-1}}$. The measured coherence spectra of all combinations can be analysed and frequency regions can be identified where the coherence drops when approaching the shear layer. As a first example the coherence

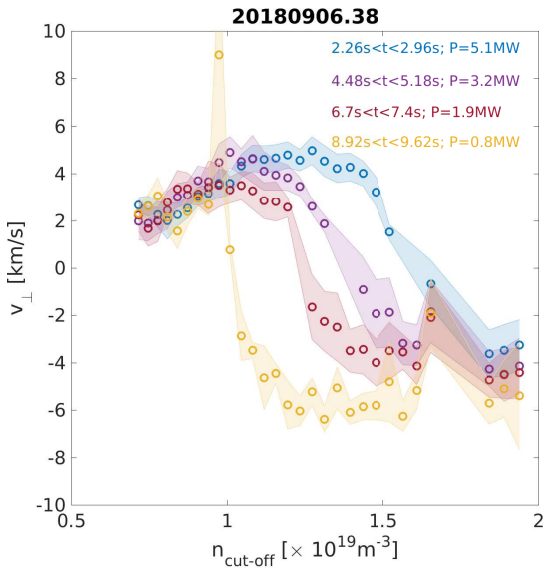

Figure 8: $v_\perp$*-profile for the standard configuration and different* P_{ECH} *levels. A clear shift of the transition from plasma edge to SOL towards smaller densities is observed with increasing* P_{ECH}.

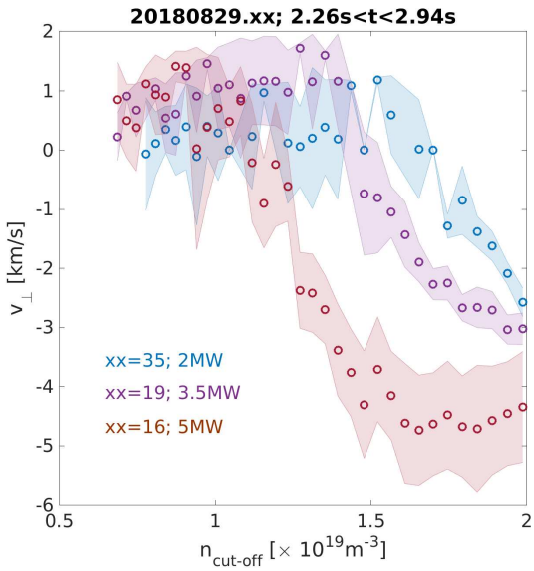

Figure 9: $v_\perp$*-profile for the low iota configuration and different* P_{ECH} *levels. A clear steepening of the shear layer and a shift towards smaller densities is observed.*

spectra for the discharge 20171109.56 are analysed for the antenna combination **DE**. In fig. 10 the $v_\perp$-profile is shown as function of the cut-off density. This discharge shows again a remnant island in the density range $0.8 \times 10^{19}\,\mathrm{m}^{-3}$ to $1.0 \times 10^{19}\,\mathrm{m}^{-3}$. Towards lower cut-off densities, in the far SOL, the rotation decreases to $1.2\,\mathrm{km\,s}^{-1}$. The shear layer is found for a density range of $1.35 \times 10^{19}\,\mathrm{m}^{-3}$ to $1.70 \times 10^{19}\,\mathrm{m}^{-3}$. In this range the velocity decreases from $v_\perp = 3.1\,\mathrm{km\,s}^{-1}$ to $v_\perp = -4.2\,\mathrm{km\,s}^{-1}$.For 5 different positions marked by coloured $\times$-symbols the coherence spectra for the antenna combination **DE** are estimated and shown in fig. 11 where the same color code is used for the spectra as for the $\times$-symbols in fig. 10. It is seen clearly that the coherence spectrum for a position inside the shear layer is broad and shows 2 quasi coherent modes at $f = \pm 25\,\mathrm{kHz}$ [18]. For the other position in side the plasma edge a decrease of the spectral intensity is observed, but, the quasi coherent peaks are still visible and change its frequency a bit. The most obvious change in the spectra happens inside the shear layer. The spectra becomes more narrow and the intensity drops significantly across the whole frequency range. A more quantitative analysis has been done by decomposing the coherence spectra. In general

4 components can be identified (i) a broad band turbulence component, (ii) two quasi coherent modes with quite narrow width and (iii) a dc component. Each component has been approached by a Gaussian shape. The whole

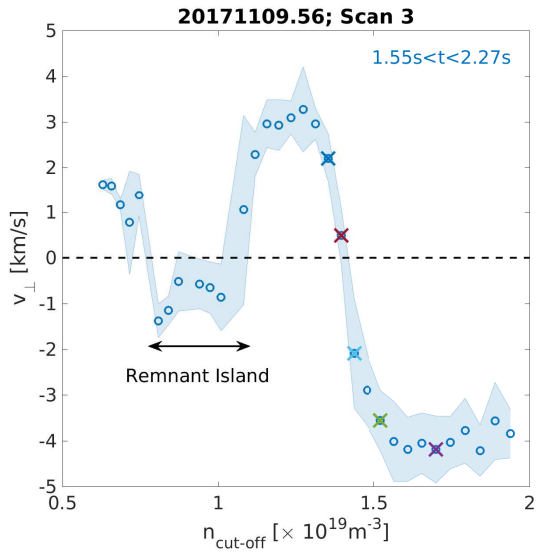

Figure 10: *$v_\perp$-profile for 20171109.56 showing the shear layer and the remnant island in the SOL. Colored × symbols denote the position at which the coherence spectra are calculated.*

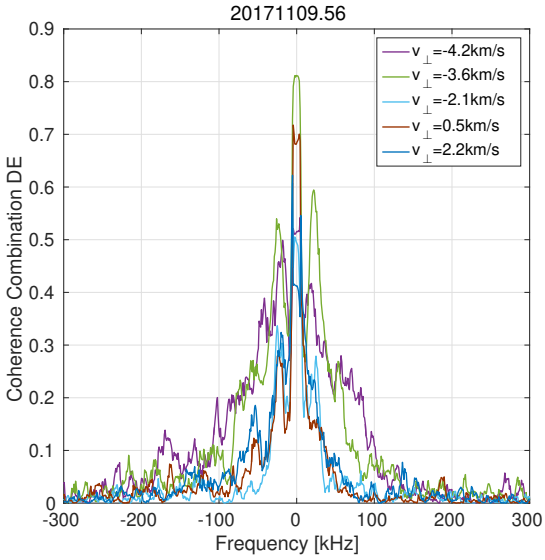

Figure 11: *Coherence spectra for positions from . A clear decrease in the broad band turbulence is seen when passing the shear layer.*

spectrum can be described as:

$$S(f) = \sum_{i=1}^{n} A_i exp\left(-\frac{(f-f_i)^2}{\sigma_i^2}\right) \tag{2}$$

where A_i denotes the amplitude of the component, f_i the centre frequency and σ_i the half width of the component. As shown in fig. 12 for the two extreme cases from fig. 11 the measured spectra can be nicely described by the sum of Gaussians. For each spectra the Gaussian components (dashed lines) are shown, except the dc component. Whereas the spectrum in the plasma edge has a strong broad band component it is missing completely in the shear layer. The quasi coherent modes components are shown as well. In contrast to the broad band turbulence the quasi coherent modes do not undergo a strong change in amplitude. This decrease of the broadband turbulence can be taken as an evidence for the suppression of low k-broad band turbulence in the shear layer.

4 Summary

During the inertial cooled divertor operation campaigns at W7-X the correlation reflectometer has been used to measure $v_\perp$-profiles in the plasma edge and the SOL. To take into account the strong velocity shear at the transition from closed to open field lines an elliptical model has been applied for the estimation of $v_\perp$. It takes into account the strongly changing width of the cross correlation function in the shear layer and avoids strong non-physical fluctuations of $v_\perp$.

In the investigated plasmas the shear layer is always located outside the LCFS as it is calculated from VMEC simulations. The shear layer is subject to changes of the magnetic configuration ($\iota = 1$ and $\iota = 0.81$) and changes of the plasma current and the heating power. Modifications of the plasma edge by the use of control coils influence the edge iota and the shear layer as well. In cases where a positive control coil current is applied the steepening of the shear layer and the movement of the shear layer to higher densities is observed. The plasma current itself increases the poloidal magnetic field and shifts the island chain to smaller radii which means more deep into the plasma. As a consequence the shear layer moves to higher densities. In none of the investigated discharges the $v_\perp$-profile inside the LCFS undergoes any change. Also the $v_\perp$-profiles in the SOL does not change when the heating power increases. However, depending on the magnetic configuration the shear layer moves towards lower cut-off densities.

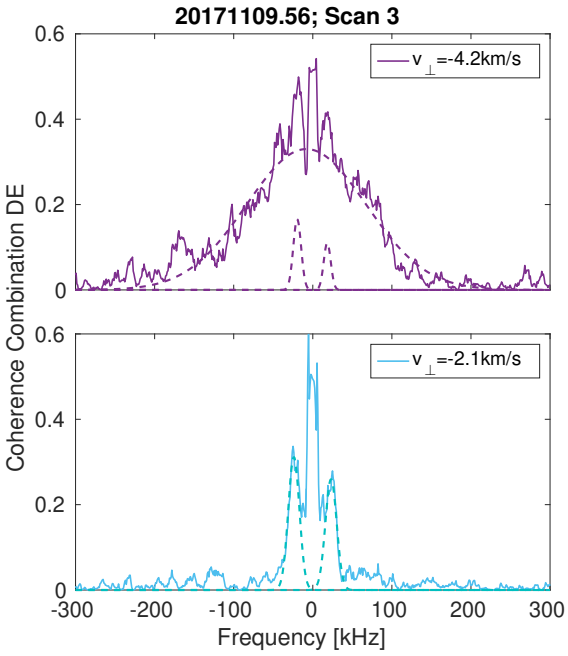

Figure 12: *Decomposition of 2 spectra into quasi coherent and broad band turbulence (dashed lines). Each spectrum has one central broad band turbulence component and 2 quasi coherent components. In the spectrum which is obtained in the shear layer the broad band turbulence vanishes completely and the quasi coherent mode is left, only.*

In case that a remnant island is observed by the PCR an increase of the plasma current seems to have no effect on the island density nor its position. However, the PCR sight line 0.1 m below the mid-plane and therefore the O-point of the island. Therefore, the effect of the plasma current on the island could become already weak.

Regarding the suppression of turbulence coherence spectra are analysed. A decomposition of the coherence spectrum in several Gaussian shaped contributions yields a significant decrease in the amplitude of the broad band turbulence in the shear layer. This is consistent with the assumption of a suppression of low k-turbulence in the shear layer.

Acknowledgement

This work has been carried out within the framework of the EUROfusion Consortium and has received funding from the Euratom research and training programme 2014-2018 and 2019-2020 under grant agreement No 633053. The views and opinions expressed herein do not necessarily reflect those of the European Commission.

References

[1] V. Naulin. Turbulent transport and the plasma edge. *Journal of Nuclear Materials*, 363-365:24?31, 2007. Plasma-Surface Interactions-17.

[2] B. Nold, P. Manz, T. T. Ribeiro, G. Fuchert, G. Birkenmeier, H. W. Mller, M. Ramisch, B. D. Scott, and U. Stroth. Turbulent transport across shear layers in magnetically confined plasmas. *Physics of Plasmas*, 21(10):102304, 2014.

[3] E.Z. Gusakov and B.O. Yakovlev. *Plasma Phys. Control. Fusion*, 44:2525–2537, 2002.

[4] B H Briggs, G J Phillips, and D H Shinn. The analysis of observations on spaced receivers of the fading of radio signals. *Proceedings of the Physical Society. Section B*, 63(2):106?121, feb 1950.

[5] G J Phillips and M Spencer. The effects of anisometric amplitude patterns in the measurement of ionospheric drifts. *Proceedings of the Physical Society. Section B*, 68(8):481?492, aug 1955.

[6] G D Conway and J A Elliott. Digital signal processing techniques for plasma dispersion curve measurements. *Journal of Physics E: Scientific Instruments*, 20(11):1341?1350, nov 1987.

[7] T Klinger, A Alonso, S Bozhenkov, R Burhenn, A Dinklage, et al. *Plasma Physics and Controlled Fusion*, 59(1):014018, 2017.

[8] R.C. Wolf, A. Ali, A. Alonso, J. Baldzuhn, C. Beidler, and et al. Major results from the first plasma campaign of the wendelstein 7-x stellarator. *Nuclear Fusion*, 57(10):102020, 2017.

[9] A. Krämer-Flecken, T. Windisch, W. Behr, G. Czymek, and P. Drews et al. Investigation of turbulence rotation in limiter plasmas at w7-x with newly installed poloidal correlation reflectometer. *Nuclear Fusion*, 57(6):066023, 2017.

[10] T Windisch, A Krämer-Flecken, JL Velasco, A Könies, C Nührenberg, and et al. Poloidal correlation reflectometry at w7-x: radial electric field and coherent fluctuations. *Plasma Physics and Controlled Fusion*, 59(10):105002, 2017.

[11] A. Krämer-Flecken, S. Soldatov, B. Vowinkel, and P. Müller. *Rev. Sci. Instrum.*, 81:113502, 2010.

[12] T. Windisch, O. Grulke, and T. Klinger. Radial propagation of structures in drift wave turbulence. *Physics of Plasmas*, 13(12):122303, 2006.

[13] B Nold, G D Conway, T Happel, H W Mller, M Ramisch, V Rohde, U Stroth, and the ASDEX Upgrade Team. *Plasma Physics and Controlled Fusion*, 52(6):065005, 2010.

[14] Guo-Wei He and Jin-Bai Zhang. Elliptic model for space-time correlations in turbulent shear flows. *Phys. Rev. E*, 73:055303, May 2006.

[15] E. Pasch et al. pages P4.016/1–4. 43rd EPS Conference on Contr. Fusion and Plasma Phys., Leuven, Belgium, 4-8 July 2016, 2016.

[16] A Krmer-Flecken, X Han, T Windisch, J Cosfeld, P Drews, G Fuchert, J Geiger, O Grulke, C Killer, A Knieps, Y Liang, S Liu, and M Rack. Investigation of turbulence rotation and radial electric field in the island divertor and plasma edge at w7-x. *Plasma Physics and Controlled Fusion*, 61(5):054003, mar 2019.

[17] S. P. Hirshman, K. C. Shaing, W. I. van Rij, C. O. Beasley, and E. C. Crume. Plasma transport coefficients for nonsymmetric toroidal confinement systems. *The Physics of Fluids*, 29(9):2951–2959, 1986.

[18] X. Han, A. Krämer-Flecken, T. Windisch, S. Liu, Y. Liang, and et al. Experimental characterization of a quasi-coherent turbulence structure in the edge plasmas in w7-x. 45th European Physical Society Conf. on Plasma Physics (Prague, Czech Republic), 2018.